Compaction, dilatancy, and failure in porous carbonate rocks

Veronika Vajdova
Department of Geosciences, State University of New York at Stony Brook, Stony Brook, New York, USA

Patrick Baud
Institut de Physique du Globe, Ecole et Observatoire des Sciences de la Terre (CNRS/ULP), Strasbourg, France

Teng-fong Wong
Department of Geosciences, State University of New York at Stony Brook, Stony Brook, New York, USA

Received 20 March 2003; revised 14 October 2003; accepted 5 February 2004; published 5 May 2004.

[1] The analysis of dilatant and compactant failure in many sedimentary and geotechnical settings hinges upon a fundamental understanding of inelastic behavior and failure mode of porous carbonate rocks. In this study we acquire new mechanical data on the Indiana and Tavel limestones, which show that the phenomenology of dilatant and compactant failure in these carbonate rocks is similar to that of the more compact Solnhofen limestone as well as sandstones. Compressibility and porosity are positively correlated. Brittle strength decreases with increasing porosity and the critical stresses for the onset of pore collapse under hydrostatic and nonhydrostatic loadings also decrease with increasing porosity. Previously, two micromechanical models were used to interpret mechanical behavior of Solnhofen limestone: viewing cataclasis and crystal plasticity as two end-members of inelastic deformation mechanisms, the wing crack and plastic pore collapse models were applied to brittle and ductile failure, respectively. Synthesizing published data for carbonate rocks with porosities between 3% and 45%, we investigate to what extent the same micromechanisms may be active at higher porosity. Application of the plastic pore collapse model indicated that crystal plasticity cannot be the only deformation mechanism. To arrive at a more realistic interpretation of shear-enhanced compaction in porous carbonate rocks cataclastic processes must be taken into account. We infer that mechanical twinning dominates in the more porous limestones and chalk, while dislocation slip is activated in the more compact limestones. *INDEX TERMS:* 5104 Physical Properties of Rocks: Fracture and flow; 5120 Physical Properties of Rocks: Plasticity, diffusion, and creep; 5112 Physical Properties of Rocks: Microstructure; 8168 Tectonophysics: Stresses—general; *KEYWORDS:* carbonate rocks, micromechanics, experimental

Citation: Vajdova, V., P. Baud, and T.-f. Wong (2004), Compaction, dilatancy, and failure in porous carbonate rocks, *J. Geophys. Res.*, *109*, B05204, doi:10.1029/2003JB002508.

1. Introduction

[2] In response to an applied stress field or pore pressure change, the pore space of a rock may compact or dilate. While dilatancy is critical for the development of brittle faulting [*Brace*, 1978], mechanical compaction induces the porosity to decrease and as a physical mechanism of diagenesis it can play an important role especially during early and intermediate burial [*Berner*, 1980; *Choquette and James*, 1986]. Mechanical compaction is also central to many problems in reservoir and geotechnical engineering. The extraction of hydrocarbon and groundwater reduces pore pressure and thus causes an increase in the effective stress in a reservoir and aquifer. For very porous or weakly consolidated formations, the increase in effective stress may be sufficient to cause inelastic deformation [*Smits et al.*, 1988; *Jones and Leddra*, 1989], and modify the stress field [*Teufel et al.*, 1991; *Segall and Fitzgerald*, 1998] as well as hydromechanical properties [*Goldsmith*, 1989; *Rhett and Teufel*, 1992; *David et al.*, 1994].

[3] The compactive deformation and failure may be spatially extensive or localized to the vicinity of the wellbore, but in either cases the consequences can be economically severe involving surface subsidence [*Boutéca et al.*, 1996; *Nagel*, 2001], induced seismicity [*Segall*, 1989; *Grasso and Wittlinger*, 1990], well failure [*Fredrich et al.*, 2000] and various production problems. Traditionally the compaction and subsidence of aquifers and reservoirs are analyzed by a poroelastic model [*Biot*, 1941; *Geertsma*, 1973], with the mechanical response characterized by an elastic modulus such as compressibility. Such an approach is limited in that it may lead to apparently contradictory predictions. Porous sandstones are considered to be more

Copyright 2004 by the American Geophysical Union.
0148-0227/04/2003JB002508$09.00

compressible than carbonate rocks, and yet a number of drastic subsidence cases have been observed in carbonate reservoirs attributed to inelastic compaction [*Nagel*, 2001].

[4] Carbonate rocks, even the ones with very low porosity like the Carrara marble, undergo the brittle to plastic transition at room temperature for confining pressures accessible in the laboratory [*Robertson*, 1955; *Paterson*, 1958; *Heard*, 1960; *Rutter*, 1974; *Fredrich et al.*, 1989]. This is due to the fact that calcite requires relatively low shear stresses to initiate mechanical twinning and dislocation slip even at room temperature [*Turner et al.*, 1954, *Griggs et al.*, 1960]. Field studies and microstructural observations have shown that inelastic deformation, pore collapse and crystal plasticity processes may be pervasive.

[5] Hence the ability to interpret and predict the occurrence and extent of deformation and failure hinges upon a fundamental understanding of the inelastic behavior, failure mode and brittle-ductile transition in porous carbonate rocks. It is now recognized that porosity change and failure mode are intimately related. On one hand, dilatancy is universally observed as a precursor to the inception of shear localization in the brittle faulting regime. On the other hand, plastic flow (associated with crystal plasticity and diffusive mass transfer) does not involve any volumetric change [*Paterson*, 1978]. In carbonate rocks the transitional regime of cataclastic flow may involve complex interplay of compaction and dilatancy, as documented by *Baud et al.* [2000] for the Solnhofen limestone with an initial porosity of 3%.

[6] We have extended the scope to investigate systematically the phenomenology and micromechanics of compaction, dilatancy and failure in three limestones with porosities ranging from 3% to 18%. We have specifically focused on several related questions. In a poroelastic model the mechanical response is characterized by an elastic modulus such as compressibility. What are the appropriate values for the rock compressibility, and to what extent can inelastic deformation be neglected in porous carbonate rocks? In carbonate rocks it has been observed that inelastic deformation, pore collapse and crystal plasticity may be pervasive. How can laboratory studies conducted under controlled conditions provide insights into the complex interplay of dilatancy and compaction, as well as failure mode? How is the damage partitioned between microcracking and crystal plasticity processes? To analyze the compactive behavior of Solnhofen limestone, *Baud et al.* [2000] interpreted their mechanical data using a model based on one end-member of deformation mechanism, crystal plasticity. To what extent is such an elastic-plastic model applicable to carbonate rocks of higher porosity? Our study focuses on limestones, but there has also been extensive investigation of chalk with porosites up to 45%. In that both limestone and chalk are carbonate rocks, do our limestone data and published data for the significantly more porous chalk follow similar trends? In this paper we will address these issues by synthesizing the laboratory data, quantitative characterization of damage and theoretical models.

2. Mechanical Data

[7] Mechanical data from this study were obtained in conventional triaxial compression tests in room temperature on vacuum dry samples. We will adopt the convention that compressive stresses and compactive strains (i.e., shortening and porosity decrease) are positive, and denote the maximum and minimum (compressive) principal stresses by σ_1 and σ_3, respectively.

2.1. Sample Material and Preparation

[8] We selected three limestones with high (>98%) calcite content for our investigation. We report here new mechanical data for the Indiana and Tavel limestones, while comprehensive data for Solnhofen limestone has recently been presented by *Baud et al.* [2000]. The Indiana limestone is fossiliferous limestone (from Bedford, Indiana) that has been investigated extensively in the rock mechanics laboratory. Previous studies on this limestone have focused on its brittle failure [*Robinson*, 1959; *Wawersik and Fairhurst*, 1970; *Zheng et al.*, 1989], mode-I fracturing process [*Hoagland et al.*, 1973; *Schmidt*, 1976; *Peck et al.*, 1985], borehole breakout [*Ewy and Cook*, 1990], indentation [*Suárez-Rivera et al.*, 1990], uniaxial strain [*Brace and Riley*, 1972], and poroelastic properties [*Hart and Wang*, 1995].

[9] The Indiana limestone consists of clasts (fossil fragments and ooids) and calcite cement resulting in a range of grain sizes from less than 5 μm for the cement to 300 μm for an average-sized fossils. In the literature porosity values for Indiana limestone have been reported to be in the range of 12% to 20%. We calculated the total porosity from the density of a vacuum dried sample assuming a solid composition of 100% calcite. Samples for 7 triaxial compression and 1 hydrostatic experiments were cored from a single block, with porosities ranging from 14.6% to 16.2% and an average of 15.6%. In addition, 2 more samples for hydrostatic experiments were cored from other blocks, with porosities 18.1% and 20.0% and designated here as Indiana18 and Indiana20, respectively.

[10] Our block of Tavel limestone is considered to be similar to samples studied previously by *Vincké et al.* [1998]. It is micritic limestone with average grain size of ~5 μm. In our samples the porosities range from 9.5% to 11.3%, with an average value of 10.4%. The Solnhofen limestone is a micritic limestone that has also been studied extensively in the rock mechanics laboratory [e.g., *Heard*, 1960; *Rutter*, 1972; *Fisher and Paterson*, 1989; *Fredrich et al.*, 1990]. The average porosity of our samples was 3.0% and the average grain size was ~5 μm [*Baud et al.*, 2000].

[11] Cylindrical samples perpendicular to the bedding were cored to diameter of 18.4 mm and length of 38.1 mm. After it had been dried in vacuum at 80°C for 48 hours, each sample was first jacketed in a thin copper foil, and then polyolefine (heat-shrinkable) tubings were used to separate the rock from the confining medium. Electric resistance strain gages (BLH SR-4 type FAE 50-12-S6 for Solnhofen and Indiana limestones, and TML type PFL 10-11 for Tavel limestone) were attached to the copper jacket to measure the axial and transverse strains. For the Tavel limestone we did not have to undertake any special jacketing procedure. However, for Indiana limestone the strain gages were easily broken due to pore collapse near the sample surface. To avoid this problem, we first pressurized the samples to

5 MPa, filled the pores near the surface with an epoxy (BLH SR-4 EPY-150) and then smoothed the surface by sanding it after the epoxy had cured. The sample was then jacketed with copper foil and strain gages were attached. For the Solnhofen limestone *Baud et al.* [2000] first "seated" the copper jacket by applying 50 MPa of confining pressure prior to gluing the strain gages.

2.2. Experimental Procedure

[12] The jacketed samples were stressed in the conventional triaxial configuration at room temperature. Kerosene was used as the confining medium. The triaxial experiments were performed at confining pressures ranging from 10 to 435 MPa for Solnhofen limestone, 10 to 240 MPa for Tavel limestone, and 5 to 50 MPa for Indiana limestone. The confining pressure was measured with accuracy of 0.1 MPa, and during triaxial loading it was held constant to within 1%. The axial load was measured with an external load cell with an accuracy of 1 kN. The displacement was measured outside the pressure vessel with a displacement transducer (DCDT) mounted between the moving piston and the fixed upper platen. The axial displacement was servo-controlled at a fixed rate (corresponding to a nominal strain rate of 1.3×10^{-5} s^{-1}).

[13] The load, displacement, and strain gage signals were acquired by a 14-bit A/D converter at a sampling rate of 1 s^{-1} with resolutions of 0.3 MPa, 1 μm and 10^{-5}, respectively. Uncertainty in strain was estimated to be 2×10^{-4} (when calculated from the DCDT signal) and 10^{-5} (when measured directly by the strain gages). The volumetric strain was calculated using the relation $\varepsilon_v = \varepsilon_{\|} + 2\varepsilon_{\perp}$, where $\varepsilon_{\|}$ and $\varepsilon_{\perp}$ are the strains measured in the axial and transverse directions, respectively. This formula is valid only for an isotropic material subjected to relatively small strains. While the transverse strains were generally small, the axial strains in some experiments exceeded 3%, and it is difficult to assess to what extent the strain gage data beyond 3% or so are reliable. Especially for the highly porous Indiana limestone, the strain gage data and axial strain inferred from DCDT data may show appreciable discrepancy at such high strains, while visual inspection of such deformed samples indicated significant grain-scale heterogeneity in deformation due to pore collapse. For these cases we prefer to use the axial strain values inferred from the DCDT data.

[14] Acoustic emission (AE) recordings were available via a piezoelectric transducer (PZT-7, 5 mm diameter, 1 MHz longitudinal resonant frequency) positioned on the flat surface of one of the end-plugs. However, during all the series of experiments that we did, no significant AE activity was resolved by our system. The AE data were not of use in this study.

2.3. Hydrostatic Compression

[15] Figure 1a shows the volumetric strain of Solnhofen limestone as a function of confining pressure. The hydrostatic response was nonlinear up to a pressure of ~200 MPa, beyond which the stress-strain curve became linear with a slope corresponding to a compressibility of $\beta = 0.016$ GPa^{-1}. Using *Walsh*'s [1965] model *Baud et al.* [2000] showed that such a hydrostat is characteristic of the response of a rock pore space made up of two types of cavities: microcracks of relatively low aspect ratios and equant pores. Progressive closure of microcracks under increasing pressure was manifested by the nonlinearity observed during initial pressurization. The data can be interpreted by the nonlinear elastic response of a pore space with ~0.2% of microcrack porosity and ~2.8% of quasi-spherical pores.

[16] Qualitatively similar behavior was observed in the Tavel limestone (Figure 1b) up to a pressure of ~290 MPa. At relatively low pressures a nonlinear "toe" was also observed, which can be attributed to the elastic closure of ~0.1% microcrack porosity. Hydrostatic compression was relatively linear at pressures between 40 MPa and 290 MPa, corresponding to a compressibility of 0.033 GPa^{-1}. Similarly hydrostatic compression of Indiana limestone (Figure 1c) was approximately linear at pressures between 10 MPa and 60 MPa corresponding to a compressibility of 0.075 GPa^{-1}, with a nonlinear "toe" at low pressures that can be attributed to the elastic closure of ~0.1% microcrack porosity.

[17] However, there is an important difference between the more compact Solnhofen limestone and the two porous limestones, in that the hydrostats of the Tavel and Indiana limestones both became nonlinear again at pressures above the critical values P^* indicated in Figures 1b and 1c. This critical pressure is identified with an inflection point in the hydrostat, and it marks the inception of pore collapse and grain crushing. While pressure cycling of an Indiana limestone sample up to 40 MPa resulted in relatively small permanent strain (~2×10^{-4}), significant inelastic volumetric strain was observed on the sample when loaded to beyond P^*. We conducted hydrostatic tests for two other samples (Indiana18 and Indiana20) from other blocks, and their hydrostats are compared in Figure 1d. In the most porous sample (Indiana20) inelastic compaction was significantly higher than in the more compact samples. Presumably the critical pressure for Solnhofen limestone is higher than the maximum pressure (of 450 MPa) considered by *Baud et al.* [2000].

[18] Traditionally compaction in reservoirs and aquifers are analyzed using poroelasticity, with compressibility as one of the key parameters. Laboratory data have shown that the compressibility is sensitive to both lithology and porosity. Limestones seem to be less compressible in comparison with sandstones of comparable porosities. In Table 1 we compiled the compressibility data for limestone and chalk with porosities ranging from 3% to 43%. Except for the compact Solnhofen limestone, the nonlinear "toe" disappeared in more porous limestones beyond a pressure of 20 MPa or so. The compressibility values in Table 1 were determined from the relatively linear portions of the hydrostats. All the limestone data are plotted in Figure 2a, and it can be seen that there is an overall trend for compressibility to increase with increasing porosity.

[19] In certain applications nonlinear elastic behavior is modeled by a pressure-dependent compressibility. In Figure 2b we differentiated the data for our three limestones to characterize this dependence. At relatively low pressures, progressive closure of microcracks induces the compressibility to decrease with pressure. Compressibility

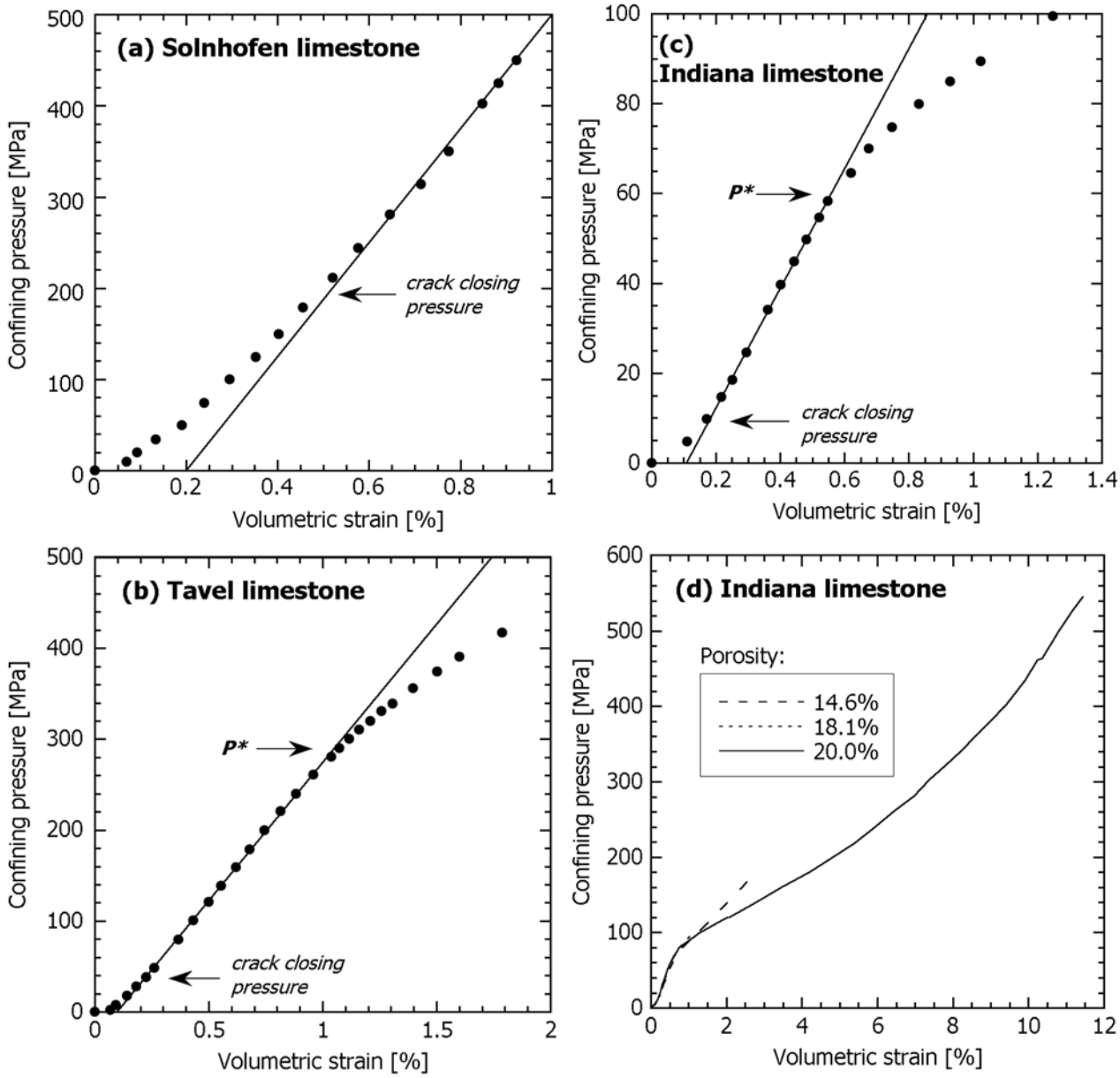

Figure 1. Mechanical data for hydrostatic experiments for (a) Solnhofen, (b) Tavel and (c) Indiana limestones as curves of confining pressure versus volumetric strain. The linear part of each curve is fitted by linear regression with zero-pressure intercept indicating crack porosity of 0.2% for Solnhofen and 0.1% for Tavel and Indiana limestones. Crack-closing pressure and pore collapse pressure P^* are indicated by arrows. (d) Hydrostatic compaction of Indiana limestone beyond the pore collapse pressure. Data for three samples from different blocks demonstrate the effect of initial porosity on the inelastic compaction behavior.

values compiled in Table 1 approximately correspond to the minimum values shown in Figure 2b. While this approach provides a realistic description of the nonlinear effects due to microcrack closure, its validity is questionable in the presence of appreciable inelastic deformation, commonly associated with pore collapse and grain crushing in porous rocks. At pressures above the critical value P^*, the apparent compressibility may increase significantly, by as much as a factor of four in the highly porous Indiana limestone. It is unlikely that a poroelastic model can then provide a mechanically realistic description of such inelastic compaction of a porous carbonate formation. A more systematic understanding of the inelastic responses is therefore necessary.

2.4. Triaxial Compression: Stress, Strain, and Porosity Change

[20] We present here the triaxial compression data for the Tavel and Indiana limestones, and compare them with data for the compact Solnhofen limestone reported by *Baud et al.* [2000]. Figure 3a shows the differential stress ($\sigma_1 - \sigma_3$) as a function of axial strain in selected experiments conducted

Table 1. Compilation of Compressibility and Critical Pressure for Carbonate Rocks Tested Under Confining Pressure

Carbonate Rock	Avg. porosity ϕ, %	Compressibility β, GPa^{-1}	Critical Pressure P^*, MPa	Saturation	Reference
Limestone					
Solnhofen	3.0	0.016	>450	dry	*Baud et al.* [2000]
Morawica	3.4	0.017	-	dry	*Fabre and Gustkiewicz* [1997]
Larrys-Mouchette	4.5	0.030[a]	-	salt water	*Laurent et al.* [1993]
Tavel	10.4	0.033	290.0	dry	this study
Bedford	11.9	0.038	-	nitrogen	*Coyner* [1984]
Indiana	13.0	0.045	-	dry	*Hart and Wang* [1995]
Tonnerre	13.7	0.052	-	dry	*Fabre and Gustkiewicz* [1997]
Vilhoneur	14.0	0.053[a]	-	salt water	*Laurent et al.* [1993]
Indiana	15.6	0.075	60.0	dry	this study
Chauvigny	17.4	0.061	140.0[a]	dry	*Fabre and Gustkiewicz* [1997]
Indiana18	18.1	0.067	60.0	dry	this study
Indiana20	20.0	-	60.0	dry	this study
Lavoux	21.8	0.072	30.0	dry	*Fabre and Gustkiewicz* [1997]
Lavoux	23.0	0.115[a]	-	salt water	*Laurent et al.* [1993]
Cordoba Cream	25.0	0.232[a]	41.4	dry	*Mowar et al.* [1994]
Louny Gaize	26.0	0.109	60.0	dry	*Fabre and Gustkiewicz* [1997]
Chalk					
Ekofisk	38.0	0.775[a]	14.0	dry	*Azeemudin et al.* [1994]
North France	39.0	0.600[a]	10.0[a]	methanol	*Dahou et al.* [1995]
Liege (Lixhe)	40.0	1.083	17.0	oil	*Risnes et al.* [1996]
Lixhe	42.0	0.263	-	dry	*Fabre and Gustkiewicz* [1997]
Lixhe	43.0	-	17.5	oil	*Homand and Shao* [2000]
Valhall	43.0	1.316	11.0	oil	*Risnes et al.* [1996]
North Sea	45.0	-	17.5	dry	*Longuemare et al.* [1995]

[a]Value inferred by us from published data of volumetric strain versus confining pressure.

on Tavel limestone at confining pressures σ_3 ranging from 10 to 240 MPa. The volumetric strain data from these experiments are plotted as a function of the mean stress $(\sigma_1 + 2\sigma_3)/3$ in Figure 3b. For reference, the hydrostat is also shown (as the dashed line) in this figure.

[21] At confining pressures of 10, 20 and 30 MPa the mechanical response and failure mode are typical of the brittle faulting regime. The differential stress attained a peak, beyond which strain softening was observed (Figure 3a). The peak stress shows a positive correlation with the confining pressure and mean stress (Table 2). The Mohr circles corresponding to the peak stresses and confining pressures can be fitted with a linear failure envelope, with cohesion 60 MPa and angle of internal friction 27°. Visual inspection of the failed samples revealed the development of localized failure subparallel to the sample axis at 10 MPa pressure, while shear bands inclined to the axis were observed in the samples faulted at higher confining

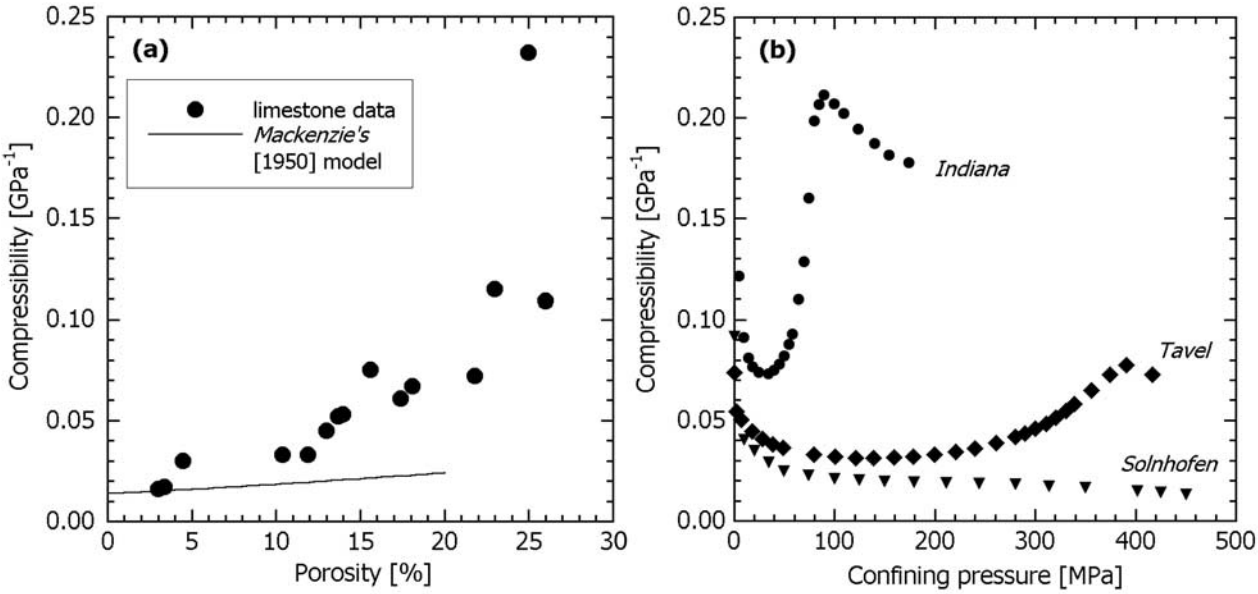

Figure 2. (a) Compilation of compressibility data on limestones. Model curve shows *Mackenzie*'s [1950] model prediction of the compressibility based on equation (1) in the text. (b) Compressibility data of three limestones as functions of confining pressure.

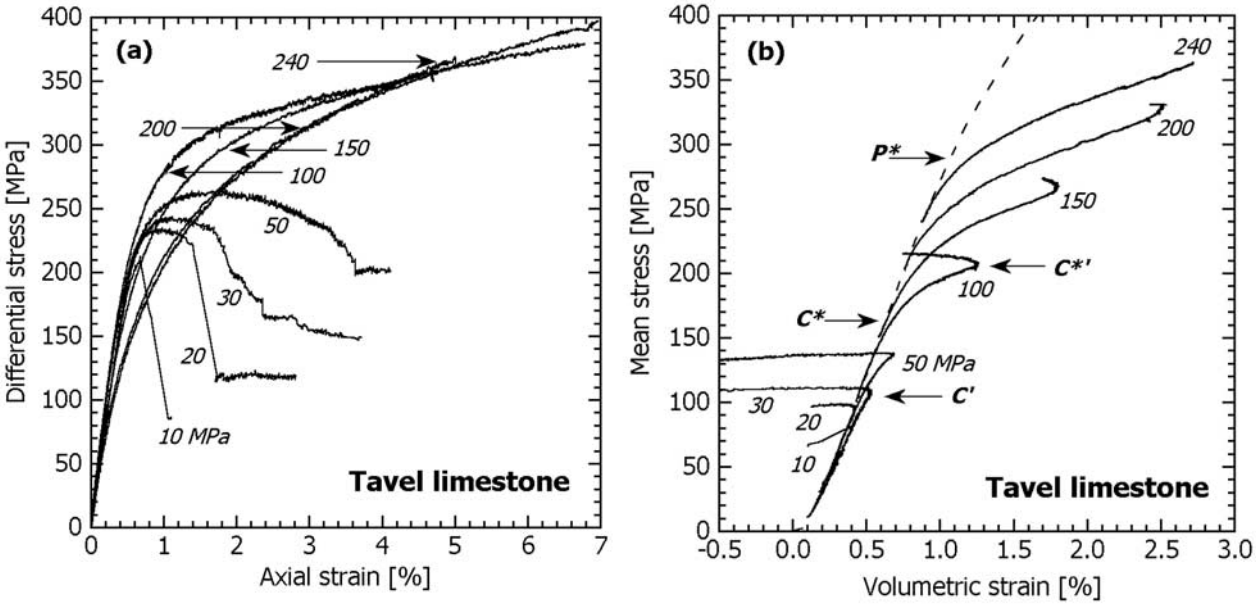

Figure 3. Representative mechanical data for selected triaxial compression experiments on Tavel limestone. (a) Differential stress is plotted versus axial strain. (b) Volumetric strain is plotted versus mean stress, and for reference the hydrostatic data are shown as the dashed line. Numbers next to each curve indicate the confining pressure maintained during the experiments. Arrows in Figure 3b mark critical stress states (onset of dilatancy C' in experiment at confining pressure of 30 MPa, onset of shear-enhanced compaction C^* and transition from shear-enhanced compaction to dilatancy $C^{*\prime}$ in experiment at confining pressure of 100 MPa).

pressures. As indicated for the experiment at confining pressure of 30 MPa, the onset of dilatancy C' can be identified on Figure 3b as the point where the volume of the triaxially compressed sample became greater than that of the hydrostatically compressed counterpart at the same mean stress. The differential stress level at C' showed a positive pressure dependence (Table 2).

[22] At confining pressures $\sigma_3 \geq 100$ MPa the initial mechanical responses are typical of the compactive cataclastic flow regime. The slopes of the differential stress-axial strain curve were nonnegative (Figure 3a). As shown in Figure 3b, the evolution of volumetric strain showed three distinct stages. The first stage was marked by the triaxial compression curve for a given confining pressure that coincided with the hydrostat up to a critical stress state (indicated by C^* for the data at 100 MPa confining pressure). At the second stage with stress levels beyond C^* there was an accelerated decrease in volume in comparison to the hydrostat. The deviatoric stress field provided significant inelastic contribution to the compactive strain, and this phenomenon in the second stage is referred to as ''shear-enhanced compaction'' [*Curran and Carroll*, 1979; *Wong et al.*, 1997].

[23] After they had undergone certain amount of strain hardening these samples consistently switched from compaction to a third stage of dilation. As indicated in Figure 3b for the experiment at 100 MPa confining pressure, the critical stress state at the transition from compactive to dilatant cataclastic flow is denoted by $C^{*\prime}$. Visual examination of the deformed samples (up to the maximum axial strain of ~7%) did not reveal any obvious signs of strain localization, even though the third stage may involve appreciable dilatancy. While the differential stress C^* at the onset of shear-enhanced compaction shows a negative pressure dependence, the differential stress at $C^{*\prime}$ shows a positive correlation with mean stress and confining pressure (Table 2). A more complex failure mode was observed at 50 MPa of confinement. A switch from shear-enhanced compaction to dilatancy was observed while the sample strain hardened. After attaining a peak stress, the sample strain softened and developed conjugate shear bands visible on the surface.

Table 2. Summary of Mechanical Data for Tavel and Indiana Limestones

Confining Pressure, MPa	C' $\sigma_1 - \sigma_3$, MPa	Peak Stress $\sigma_1 - \sigma_3$, MPa	C^* $\sigma_1 - \sigma_3$, MPa	$C^{*\prime}$ $\sigma_1 - \sigma_3$, MPa
		Tavel Limestone		
10	194	211	-	-
20	204	232	-	-
30	215	242	-	-
50	-	263	207	261
100	-	-	189	320
150	-	-	165	352
200	-	-	127	393
240	-	-	90	-
		Indiana Limestone		
5	34	45	-	-
10	40	52	-	-
20	-	-	41	77
30	-	-	38	88
40	-	-	29	97
50	-	-	19	101

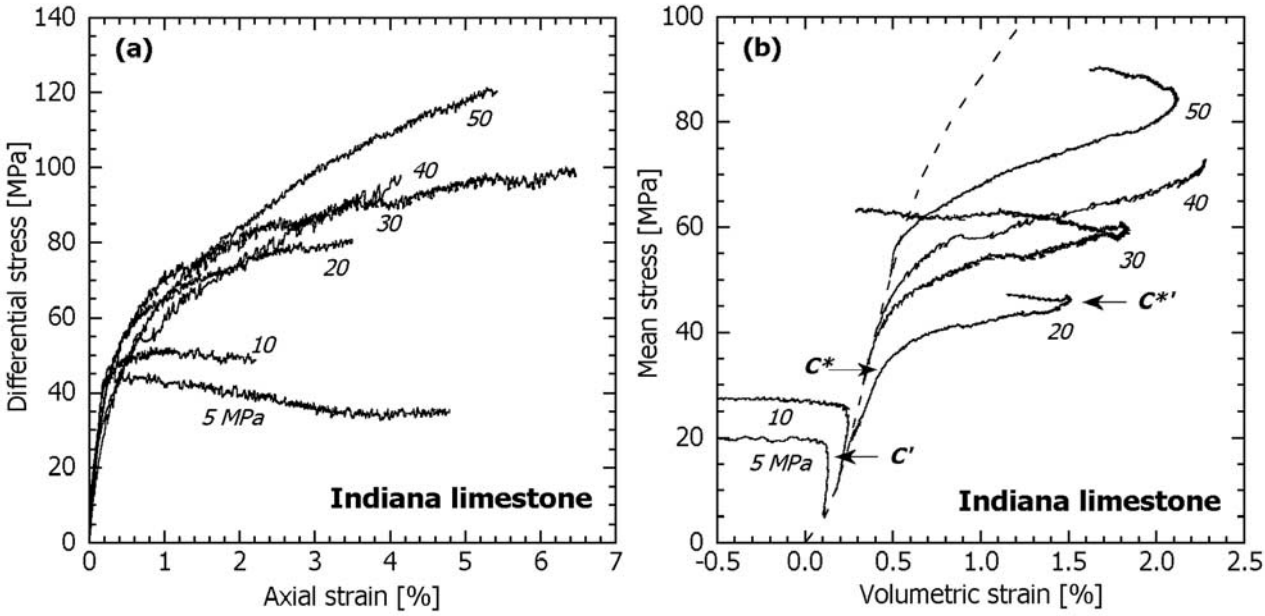

Figure 4. Representative mechanical data for selected triaxial compression experiments on Indiana limestone. (a) Differential stress is plotted versus axial strain. (b) Volumetric strain is plotted versus mean stress, and for reference the hydrostatic data are shown as the dashed line. Numbers next to each curve indicate the confining pressure maintained during the experiments. Arrows in Figure 4b mark critical stress states (C' in experiment at confining pressure of 5 MPa, C^* and $C^{*\prime}$ in experiment at confining pressure of 20 MPa).

[24] Qualitatively similar mechanical behavior was observed in Indiana limestone. At 5 MPa and 10 MPa of confining pressure the Indiana limestone samples failed by brittle faulting accompanied by dilatancy and strain softening (Figures 4a). The Mohr circles corresponding to the peak stresses and confining pressures can be fitted with a linear failure envelope, with cohesion 12 MPa and angle of internal friction 28°. The failure localized along a well-defined shear plane at 5 MPa, but at 10 MPa the shear plane was not as clearly developed. Compactive cataclastic flow occurred at pressures of 20 MPa and higher, accompanied by strain hardening and a switch from shear-enhanced compaction to dilatancy in the last stage (Figure 4b). The critical stress data for Indiana limestone are compiled in Table 2. The mechanical behavior of Solnhofen limestone of *Baud et al.* [2000] is qualitatively similar to that of Tavel and Indiana limestone.

3. Discussion

[25] Quantitative extrapolations of the laboratory data to crustal settings would require a fundamental understanding of the micromechanics of the brittle-ductile transition, which cannot be formulated without a realistic conception of the pore geometry and defect structure. We emphasized above that from a phenomenological perspective the mechanical deformation and failure mode of the three limestones with porosities ranging from 3% to 16% are very similar. For the Solnhofen limestone, *Baud et al.* [2000] concluded that the compressibility and shear-enhanced compaction behavior of this relatively compact rock can be interpreted satisfactorily by the elastic deformation and plastic collapse of isolated spherical pores embedded in a solid calcite matrix. They also concluded that the brittle faulting behavior can be explained by a sliding wing crack model. Since we have acquired new data and expanded the range of porosities, a first question we would like to address is to what extent these micromechanical models remain applicable to the more porous limestones.

3.1. Effect of Porosity on Compressibility

[26] *Baud et al.* [2000] showed that the linear portion of the Solnhofen limestone hydrostat (Figure 1a) can be modeled as the hydrostatic response of a void space made up of relatively equant pores with a porosity of ~2.8% (equal to the difference between the total and microcrack porosity). Specifically they used *Walsh*'s [1965] model for the effective compressibility β_{eff} of an elastic matrix embedded with a dilute concentration of spherical pores:

$$\frac{\beta_{eff}}{\beta} = 1 + \frac{3}{2}\frac{(1-\nu)}{(1-2\nu)}\frac{\phi}{(1-\phi)} \tag{1}$$

where ϕ is the porosity of the equant pores, and β and ν are the intrinsic compressibility and Poisson's ratio, respectively, of the solid (calcite) grain. For a calcite aggregate the Reuss averages for the intrinsic elastic moduli are β = 0.014 GPa^{-1} and ν = 0.335 [*Simmons and Wang*, 1971]. It should be noted that there is a typographical error in equation (1a) of *Baud et al.* [2000]: in the denominator on the right hand side the expression $1 + \phi$ should be $1 - \phi$.

[27] At higher porosities, it is inappropriate to assume the concentration of pores to be dilute and one should consider

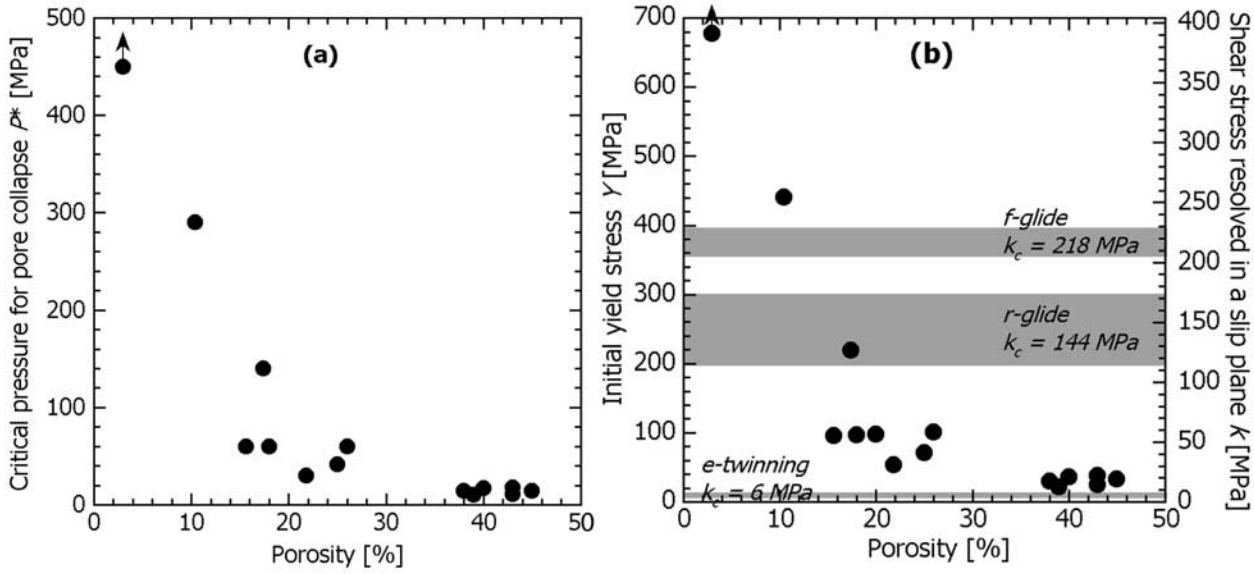

Figure 5. (a) Compilation of pore collapse pressure for carbonate rocks. (b) Yield stresses Y inferred from P^* data for carbonate rocks using equation (3). Axis on the right provides a reference to the resolved shear stresses k required for activation of crystal plasticity. The data of *Turner et al.* [1954] on critical stresses k_c for activation of twinning and dislocation slip are represented by the shaded zones embracing their average values of 6, 144 and 218 MPa for mechanical *e*-twinning, *r*-glide and *f*-glide, respectively, at room temperature.

a model that accounts for interaction among the pores. If the pore geometry can still be approximated as spherical, one can use *Mackenzie*'s [1950] variation of the self-consistent method as long as $\phi^2 \ll 1$. The Mackenzie's approximation turns out to give an expression identical to equation (1) which is shown as the solid curve in Figure 2a in the porosity range from 0 to 20%.

[28] While there is reasonable agreement with the experiment data for the two most compact limestones (Solnhofen and Morawica limestones with porosities of 3.0% and 3.4%), significant discrepancy exists for the more porous limestones. The total porosity was used for the experimental data, but as noted above the crack porosity in a porous limestone is relatively small and not expected to contribute to such a pronounced discrepancy. There are other models based on the self-consistent and differential schemes [*Walsh*, 1980; *Zimmerman*, 1991] but it is unlikely that they can provide better agreement with the data of the more porous limestones. That they are more compressible than what the model predicts is possibly because the pore geometry cannot be idealized as spherical except for the most compact end-members. A model is desirable that appropriately accounts for pore interaction as well as non-spherical pore geometry such as model suggested, for example, by *Kachanov* [1994].

3.2. Effect of Porosity on the Critical Pressure for Onset of Pore Collapse

[29] At pressures above the critical value P^* (Figures 1b, 1c, 1d) inelastic processes associated with pore collapse result in enhanced compaction. The phenomenological behavior in the porous limestones is similar to that observed in sandstone, tuff and chalk [*Bhatt et al.*, 1975; *Zhang et al.*, 1990]. In Table 1 we have compiled P^* data for limestone and chalk with porosities ranging from 3% to 45%. In sandstones the onset of pore collapse and grain crushing is manifested by a surge of AE activity, and the critical pressure P^* can therefore be determined from a combination of mechanical and AE data. In limestones the AE events are relatively few and one has to depend solely on the inflection point of the hydrostat for such a determination. As a result there seems to be more scatter and uncertainty in the critical pressure data for carbonate rock when compared with sandstone.

[30] Studies on chalks saturated with various fluids indicate that the critical pressure decreases in the presence of chemically reactive fluid [*Risnes et al.*, 1996; *Homand and Shao*, 2000]. We compile in Table 1 P^* data only for carbonate rock samples which were either dry or saturated with nonreactive fluids. There is an overall trend for the critical pressure to decrease with increasing porosity (Figure 5a): a significant decrease of P^* was observed in the porosity range of 3% to 15%, whereas a more gradual decrease occurs in the range of 15% to 45%.

[31] *Wong et al.* [1997] compiled laboratory data for sandstone, sand, glass beads and volcanic tuff with porosities ranging from 7% to 52%. They observed that the critical pressure is related to the initial porosity and grain radius in accordance with the Hertzian fracture model of *Zhang et al.* [1990]. However, *Baud et al.* [2000] argued that since pore collapse in the Solnhofen limestone seems not to involve appreciable grain-scale cracking, a more appropriate model would be that of *Curran and Carroll* [1979] that appeals to plastic collapse of spherical pores. How do the carbonate rock data compare with the two models?

[32] If the rock's porosity is low and the pore dimensions are sufficiently small one can model a representative element volume as an isolated thick-walled spherical shell

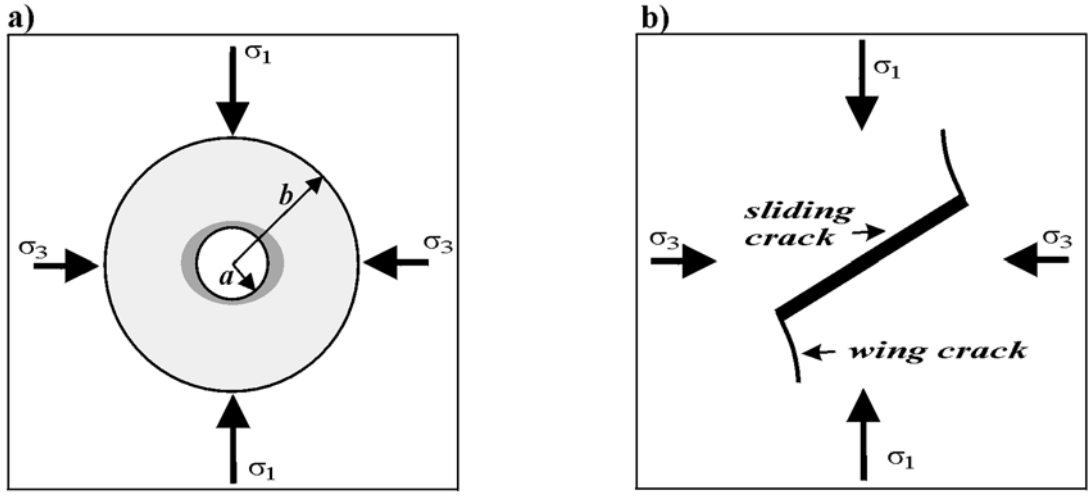

Figure 6. Two conceptual models of failure micromechanisms. (a) Plastic collapse of an isolated spherical pore may account for inelastic compaction. Dark-gray zone represents the initiation of plastic deformation while the remaining volume (light-gray) experiences elastic deformation. (b) Dilatancy and brittle faulting were explored by wing crack model.

(Figure 6a) of inner radius a and outer radius b. To relate the local geometry to the porosity ϕ, the radii a and b are chosen such that $\phi = (a/b)^3$. The applied stress field induces stress concentration in the vicinity of the spherical pore, and permanent deformation occurs if the local stress field σ_{ij} satisfies a specified yield condition. In their elastic-perfectly plastic model, *Curran and Carroll* [1979] adopted the von Mises yield criterion

$$\sqrt{J_2} = k = Y/\sqrt{3}, \tag{2}$$

where $J_2 = [(\sigma_{11} - \sigma_{22})^2 + (\sigma_{22} - \sigma_{33})^2 + (\sigma_{33} - \sigma_{11})^2]/6 + \sigma_{12}^2 + \sigma_{13}^2 + \sigma_{23}^2$ is the second invariant of the deviatoric stress tensor. The parameters k and Y correspond to the plastic yield stresses for pure shear and uniaxial tension (or compression), respectively. For hydrostatic loading this model [*Carroll*, 1980] predicts that initial yield (corresponding to the onset of plastic collapse) occurs at the macroscopic critical pressure

$$P^* = \frac{2}{3} Y \left[1 - \left(\frac{2\mu\phi}{2\mu + Y(1-\phi)} \right) \right] \tag{3}$$

where μ is the shear modulus and ϕ the initial porosity. For a calcite aggregate the Reuss average for the shear modulus is $\mu = 26.9$ MPa. If critical pressure and porosity values from Table 1 are substituted into equation (3), this spherical pore collapse model predicts that the yield stresses Y would decrease with increasing porosity as shown in Figure 5b. For reference the critical resolved shear stresses for three crystal plasticity mechanisms (*e*-twinning, *r*-glide, *f*-glide) at room temperature are also indicated in Figure 5b.

[33] One plausible interpretation of the critical pressure data and the apparent decrease of yield stress with increasing porosity is that different crystal plasticity processes were activated in the two porosity ranges. On one hand, the relatively low yield stress values inferred from equation (3) for the porosity range of 15–45% are comparable to the shear stresses required to activate *e*-twinning in calcite [*Turner et al.*, 1954; *Griggs et al.*, 1960]. *Groshong* [1974] reported significant twinning in an Indiana limestone sample (of initial porosity of 13.4%) that had been hydrostatically compacted to 100 MPa, and his conclusion is corroborated by our own microstructural observations that will be detailed in a future publication. Hence pore collapse that initiates at the critical pressure P^* involves mechanical twin gliding, and the local stress concentration should exceed the minimum value of ~10 MPa to activate *e*-twinning in calcite [*Turner et al.*, 1954].

[34] On the other hand, in the lower porosities (<15%), the relatively high yield stresses are comparable to those associated with dislocation slip processes. Indeed, for the Solnhofen limestone with 3% porosity *Baud et al.* [2000] have suggested that since the von Mises requirement of five independent slip systems represents a necessary condition for macroscopic flow in the vicinity of a spherical pore, multiple slip systems (some of which are not favorably oriented) need to be activated at very high yield stresses. Unlike mechanical twinning dislocation slip is thermally activated, and therefore if plastic yield in the more compact limestones indeed arises from such a mechanism the yield stress is expected to be sensitively dependent on temperature.

[35] It should be also noted that grain size may influence the activation of crystal plasticity processes. While Indiana limestone is fossiliferous with relatively large grain size and belongs to the higher porosity group, Tavel and Solnhofen limestones are both micrites and belong to the lower porosity group. Our inference about twinning activity in the higher porosity group is possibly related to the experimental finding that twinning is inhibited in fine-grained rocks [*Rowe and Rutter*, 1990].

[36] Other petrophysical characteristics such as pore shape or cementation type are also likely to affect the mechanical behavior. As suggested by one reviewer (F. Chester), chalk and tight limestone like Solnhofen must have grain structure different from that of limestones like Indiana where fossils and pellets are possibly similar to

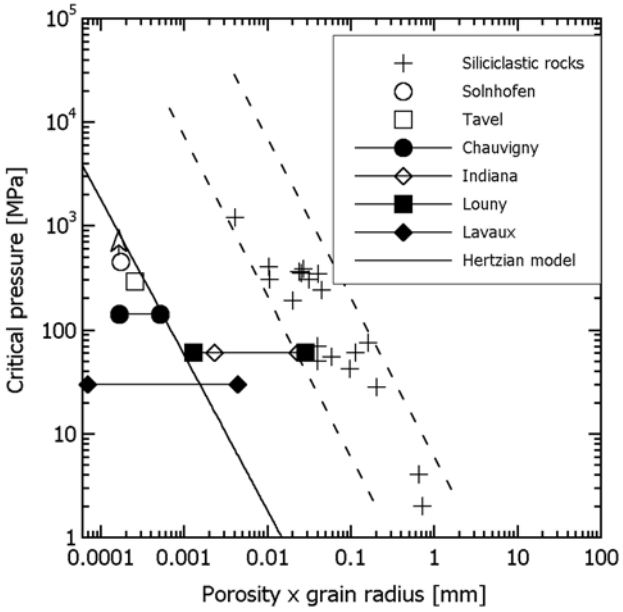

Figure 7. Critical pressure P^* for the onset of grain crushing under hydrostatic loading as a function of the product of initial porosity and grain radius. Open symbols represent data of Solnhofen, Tavel, and Indiana limestones from *Baud et al.* [2000] and this study, dark symbols represent data from *Fabre and Gustkiewicz* [1997]. The solid trend line is a prediction of the Hertzian fracture model using parameters as described in the text. Two dashed lines bracket data of siliciclastic rocks from *Wong and Baud* [1999].

granular aggregates with Hertzian stress risers. The geometric effect of different pore structure and grain size may be responsible for a change in microscopic deformation mechanisms. Unfortunately we do not have the petrophysical information detailed enough to validate this hypothesis.

[37] Next we compare our limestone data to the Hertzian fracture model where the yield is expected to arise from fractures due to impinging neighboring grains. In siliciclastic porous materials *Wong et al.* [1997] observed that the critical pressure P^* is related to the porosity ϕ and grain radius R in accordance with the relation $P^* \propto (\phi R)^n$ with $n \approx -3/2$ as predicted by *Zhang et al.* [1990]. The application of the model to limestone is complicated by the wide distribution of grain sizes among micrite, sparite and bioclasts making it hard to determine the representative grain size value. Data for Solnhofen, Tavel and Indiana limestones are shown as empty symbols in Figure 7. Values of (ϕR) corresponding to the average grain radius for Solnhofen and Tavel limestones (2.5 μm) and a range of grain radii between sparite cement (15 μm) and bioclasts (150 μm) for Indiana limestone were used. Three other limestones from the study of *Fabre and Gustkiewicz* [1997] are shown as dark symbols, corresponding to the values of grain radius they reported. For reference data on siliciclastic material compiled by *Wong and Baud* [1999] are bracketed by the two dashed lines with the characteristic slope of $-3/2$ for Hertzian fracture model. The limestone data do not follow such a trend. The apparent discrepancy may arise simply because Hertzian fracture is not important as a micromechanism for initiating pore collapse. However, our microstructural observations (V. Vajdova, N. Chen, and T.-f. Wong, Micromechanics of dilatant and compactive failure in two limestones, manuscript in preparation, 2004) on Indiana limestone indicate Hertzian fracture especially in some sparry grains. Nevertheless, it is unlikely that Hertzian fracture model as developed by *Zhang et al.* [1990] applies directly to a rock with highly heterogenous grain structure. Their model considers that the grains have ideal elastic and fracture mechanics properties, as well as uniform defect structure (characterized by a constant ratio c/R, where c is the length of the preexisting cracks in calcite grains). Most probably these rather restrictive assumptions do not apply simultaneously to the fossils and sparite in the Indiana limestone. For reference we show in Figure 7 as solid line the model prediction given by equation (7) of *Zhang et al.* [1990] for $c/R = 2 \times 10^{-2}$, fracture toughness $K_{IC} = 0.26$ MPa·m$^{1/2}$ (see section 3.4) and elastic moduli as given here in section 3.1. To summarize, neither of the two end-member models tested here can fully explain the laboratory measurements. It is desirable to develop a model that can simultaneously account for crystal plasticity and cataclastic processes.

3.3. Interplay of Compaction and Dilatancy During Cataclastic Flow

[38] In the previous study *Baud et al.* [2000] demonstrated that shear-enhanced compaction and pore collapse were readily observed in Solnhofen limestone with an initial porosity as low as 3%. This implies that pore collapse is a fairly common deformation process that can occur even in rocks considered to be relatively compact. However, it should be noted that such compactive deformation may be transient in nature. As mapped in the stress space (Figures 8a, 8b and 8c), the yield stresses for shear-enhanced compaction in all three limestone are initially described by a compactive yield envelope with negative slope that expands with strain hardening, gradually evolving to a dilatant yield envelope with positive slope.

[39] Our data here confirm that this phenomenon of compaction as a transient precursor leading to dilatancy is generally observed in porous carbonate rocks. It is therefore inappropriate to view stress-induced compaction and dilatancy as mutually exclusive processes, especially when large strains are involved, as in many geological field settings. Our experiments were conducted up to a maximum axial strain of ~7%. It is conceivable that more complex behavior would occur if deformation was to develop to even larger strains. The brittle-ductile transition is associated with a broad spectrum of highly complex deformation mechanisms, failure modes, and fluid transport processes. While dilatant cataclastic flow may be a transient precursor for the inception of shear localization and brittle faulting, shear-enhanced compaction may also evolve to dilatant cataclasis. Extrapolation of our laboratory data to the temporal and spatial scales of geologic settings would require a fundamental understanding of the micromechanics of the brittle-ductile transition, which may involve the complex interplay of microcracking, crystal plasticity, and diffusive mass transfer processes.

3.4. Development of Dilatancy and Brittle Faulting

[40] Dilatancy in a brittle rock has been observed to arise from intra and inter-granular cracking with a preferred

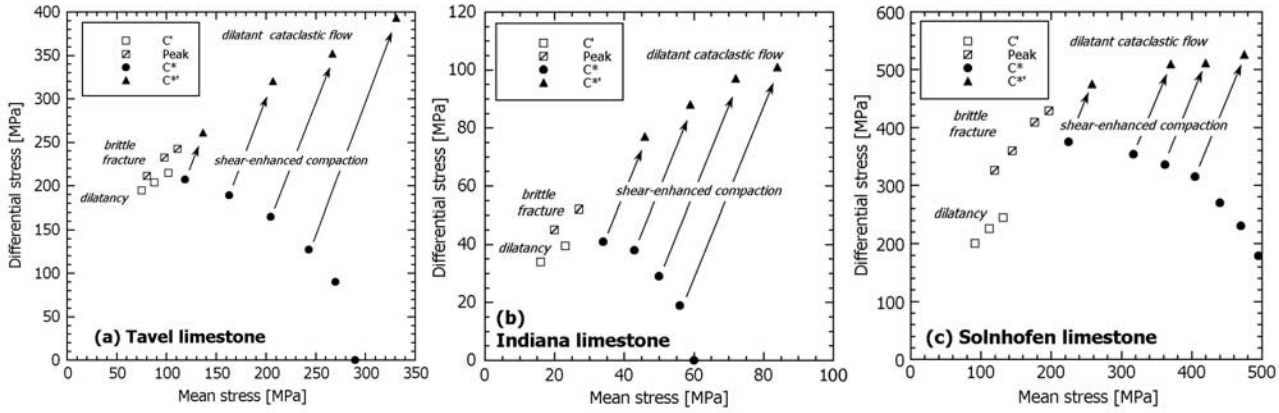

Figure 8. Stress states C, C^* and $C^{*\prime}$ and peak stress are shown in the stress space for (a) Tavel (b) Indiana, and (c) Solnhofen limestone. Three regimes of inelastic failure can be identified: brittle fracture, dilatant cataclastic flow, and shear-enhanced compaction.

orientation for propagation parallel to σ_1. In the strain softening stage, microcracking activity localizes along a macroscopic shear band [*Tapponier and Brace*, 1976; *Wong*, 1982; *Fredrich et al.*, 1989]. A conceptual model widely used to analyze such micromechanical processes is the sliding crack (Figure 6b) [*Horii and Nemat-Nasser*, 1986; *Ashby and Sammis*, 1990; *Kemeny and Cook*, 1991]. The applied far-field stresses induce a shear traction across the faces of a preexisting crack (of length $2a$). If the resolved shear traction exceeds the frictional resistance on the closed crack surface, frictional slip occurs which also induces tensile stress concentrations at the two tips and may induce wing cracks to nucleate and extend out of the plane of the preexisting crack. The driving force is characterized by the stress intensity factor K_I at the tip of the putative wing crack. With increased loading, it will attain the critical value K_{IC}, at which point the wing crack nucleates and propagates along a curved path to ultimately reach a stable orientation parallel to the direction of σ_1.

[41] We applied the wing crack model to our data in the brittle faulting regime in the same manner as *Baud et al.* [2000]. If the onset of dilatancy C' is identified with the initiation of wing cracks then a linear relation exists between the remotely applied principal stresses [*Cotterell and Rice*, 1980] as expressed by equation (2) of *Baud et al.* [2000]. To analyze the peak stress, we adopted *Ashby and Sammis*'s [1990] two-dimensional (plane strain) model where remotely applied principal stresses are predicted to evolve with accumulated damage in accordance with their equation (17) (rewritten in our sign convention as equation (3) of *Baud et al.* [2000]). Figure 9 summarizes the application of the wing crack model to our data. Model predictions for onset of dilatancy and peak stresses are compared with our mechanical data for Indiana and Tavel limestones.

[42] Typically in a micromechanical model idealized assumptions must be made so that the mathematical analysis is tractable. In a real rock the stress concentration mechanism and crack geometry are expected to be more complex than envisioned in the sliding wing crack model. Nevertheless, if the same model is applied to several rocks of similar lithology, the inferred frictional and fracture mechanics parameters can provide relative indicators of failure behavior.

[43] The three parameters (the initial damage D_o, friction coefficient, and normalized fracture toughness $K_{IC}/(\pi a)^{1/2}$ used to fit our data in Figure 9 are compiled in Table 3, which also includes the results of *Baud et al.* [2000] for the Solnhofen limestone. If we assume that the sliding crack length ($2a$) is comparable to the average grain size then K_{IC} can also be inferred. From Table 3 it can be seen that the inferred values of K_{IC} for the Tavel, Indiana and Solnhofen limestones are comparable to the value of 0.19 MPa·m$^{1/2}$ measured for crack propagation in calcite along the (1011) plane [*Atkinson and Avdis*, 1980]. Our

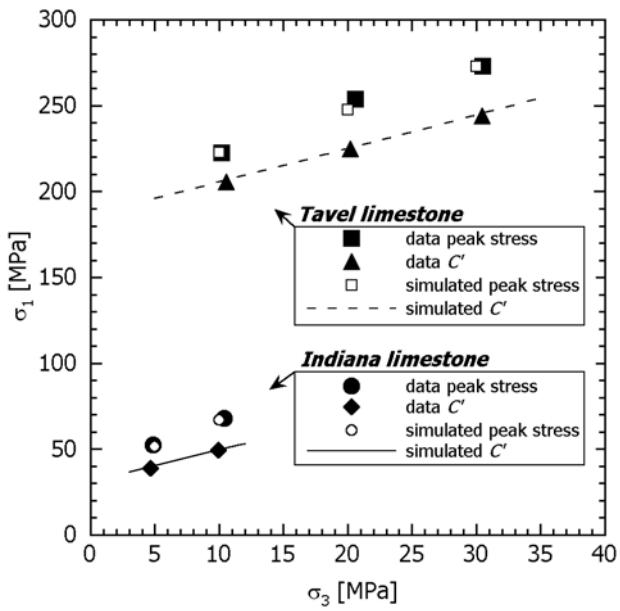

Figure 9. Comparison of the experimental data on brittle faulting (onset of dilatancy C' and the peak stress) for Indiana and Tavel limestones with predictions based on wing crack model. The relevant parameters are compiled in Table 3. Equations (2) and (3) of *Baud et al.* [2000] were used to fit the onset of dilatancy C' and the peak stress, respectively.

Table 3. Summary of Parameters Inferred From Application of Wing Crack Model and Plastic Pore Collapse Model

Limestone	Friction Coefficient	$K_{IC}/(\pi a)^{1/2}$, MPa	D_0	$2a$, mm	K_{IC}, MPa.m$^{1/2}$	Y Inferred from P*, MPa	Y Inferred from C*, MPa
Indiana	0.32	13	0.17	0.300	0.28	106	134
Tavel	0.34	77	0.28	0.005	0.22	485	580
Solnhofen[a]	0.53	97	0.25	0.005	0.27	-	975

[a]Values from *Baud et al.* [2000].

values are somewhat higher, which may reflect the fact that the (1011) plane corresponds to the easiest cleavage in calcite. The friction coefficients inferred for the more porous limestones are much lower than that for Solnhofen limestone. A relatively low friction coefficient of 0.3 for the Indiana limestone was also obtained by *Myer et al.* [1992] in their wing crack model. In the absence of a more systematic study it is not possible to conclude whether this reflects a systematic trend.

[44] Porosity also seems to influence the brittle strength of carbonate rocks. The data in Figure 10 have been obtained from triaxial compression experiments on carbonate rocks with initial porosities ranging from 1.7% to 43%. Our compilation indicates a systematic trend for the peak stress to decrease with increasing porosity. It is of interest to note that a similar trend has been documented for porous siliciclastic rocks [*Vernik et al.*, 1993].

3.5. Onset and Development of Shear-Enhanced Compaction: Micromechanics of Pore Collapse

[45] Our experimental investigation of the onset and development of shear-enhanced compaction have focused on three limestones. However, the phenomenology described here applies generally to a broad range of porous carbonate rocks. This is illustrated in Figures 11a and 11b, where we compiled representative data for the yield caps of 5 porous carbonate rocks with porosities ranging from 3 to 43%. In section 3.2 we focused on hydrostatic loading and compared the mechanical data for the onset of pore collapse with predictions of the plastic pore collapse and the Hertzian fracture models. Here we will analyze the yield behavior under nonhydrostatic loading and compare the data with model predictions on the onset of shear-enhanced compaction.

[46] As before a dilute concentration of spherical pores embedded in a solid calcite matrix will be considered in the plastic collapse model. If such a porous rock is subjected to conventional triaxial compression, permanent deformation initiates locally at the circular perimeter of the spherical pore that is parallel to σ_3. Initial yield occurs when the remotely applied stresses satisfy a critical condition that is specific to the yield criterion. For the von Mises criterion (2) the critical condition was given by equation (6) of *Baud et al.* [2000], who used it to analyze the yield behavior in Solnhofen limestone due to pressure-insensitive dislocation slip. *Curran and Carroll* [1979] have shown that initial yield occurs if the mean stress $P = (\sigma_1 + 2\sigma_3)/3$ and differential stress $Q = \sigma_1 - \sigma_3$ satisfy the critical condition

$$\left[9RP^2 + SP(3P - Q) + (U + V + 3W)(P - Q/3)^2 + 2WPQ\right]^{1/2} = k = Y/\sqrt{3} \quad (4)$$

where the coefficients R, S, U, V and W depend on the elastic moduli and the ratio a/b (and therefore the porosity). *Baud et al.* [2000] provided explicit expressions for these five coefficients in their appendix.

[47] *Baud et al.* [2000] have concluded that *Curran and Carroll*'s [1979] model with the von Mises yield condition (2) provides a reasonable fit to the C^* data of Solnhofen limestone. Figure 12a and 12b compare the predictions of this model with our new data for the Tavel and Indiana limestones. Porosity and elastic moduli values used in the calculation are as indicated in the figures. For each rock we calculated two envelopes that bracket the mechanical data for C^*. For the first envelope we used equation (3) to infer the yield stress Y from the pore collapse pressure P^*, and then substituted these inferred values (106 MPa and 485 MPa for the Indiana and Tavel limestones, respectively) into equation (4). The model consistently underestimates the differential stress required to initiate shear-enhanced compaction: while this first envelope fits the hydrostatic data P^*, it consistently falls below the experimental mea-

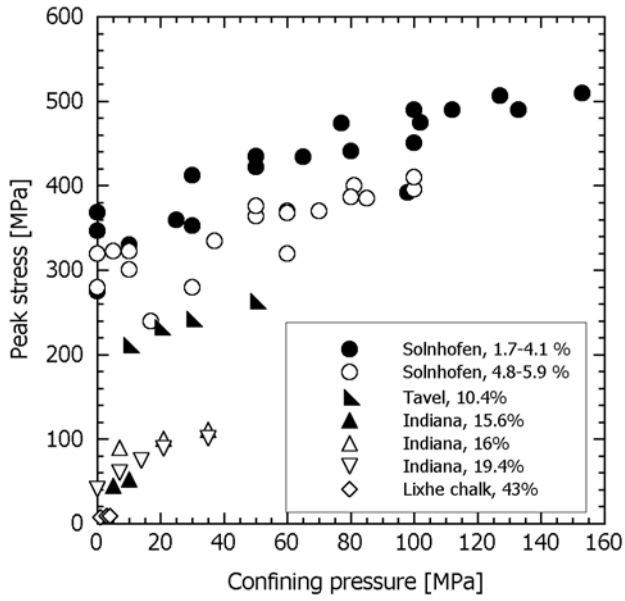

Figure 10. Compilation of peak stress data for carbonate rocks of different porosities. (Initial porosity in per cent is indicated for each rock.) Data sources: Solnhofen limestone: compilation in *Baud et al.* [2000]; Tavel limestone, 10.4%: this study; Indiana limestone, 15.6%: this study; Indiana limestone, 16.0%: *Boozer et al.* [1962]; Indiana limestone, 19.4%: *Schwartz* [1964]; Lixhe chalk: *Homand and Shao* [2000].

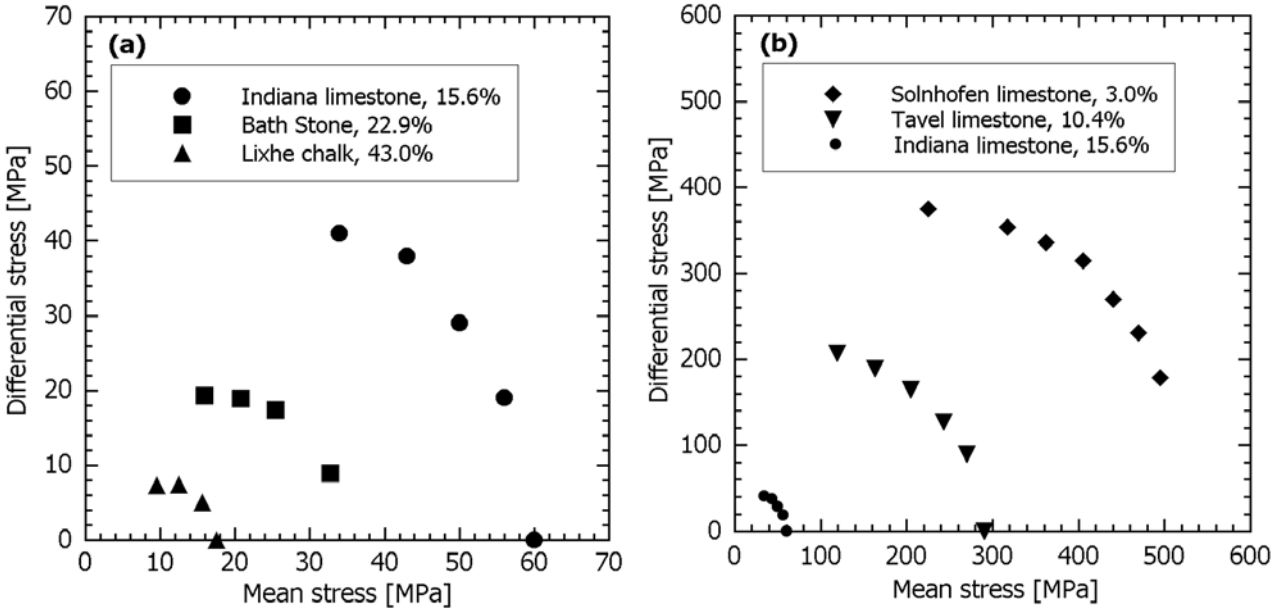

Figure 11. Compilation of compactive cataclastic flow yield envelopes for carbonate rocks of (a) high and (b) low porosities. For reference, Indiana limestone appears in both graphs. Initial porosity in per cent is indicated for each rock. Data sources: Lixhe chalk: *Homand and Shao* [2000]; Bath Stone: *Elliot and Brown* [1986]; Indiana limestone: this study; Tavel limestone: this study; Solnhofen limestone: *Baud et al.* [2000].

surement of C^*. To calculate the second envelope we adjusted the Y value until we arrived at an optimal fit to the triaxial compression data C^*. Values of the yield stresses Y are summarized in Table 3. For the two limestones, in order to match the shear-enhanced compaction data the yield stresses have to be increased relative to the values inferred from P^*, and the envelopes so obtained are shown as the upper curves in Figure 12a and 12b.

[48] Our comparison here shows that *Curran and Carroll*'s [1979] model (based on pressure-independent yielding) can capture the compactive yield behavior under nonhydrostatic loading. The value of the yield stress Y (required to fit the cap for the onset of shear-enhanced compaction) decreases with increasing porosity, and our previous interpretation (based on analysis of the hydrostatic data) that different crystal plasticity mechanisms are operative provides a plausible micro-

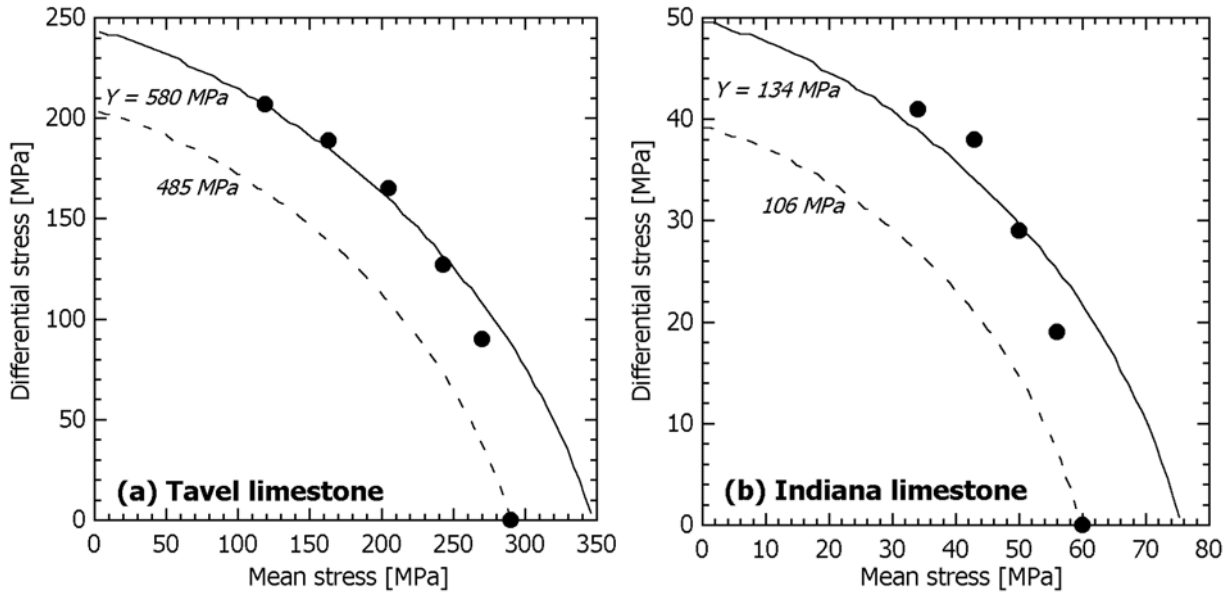

Figure 12. Initial yield envelopes for (a) Tavel and (b) Indiana limestone assuming matrix material governed by von Mises yield criterion calculated using the model of *Curran and Carroll* [1979]. The solid points represent C^* data outlining the cataclastic flow envelope, solid curve represents the best fit to the C^* data and dashed curve the fit of solely the pore collapse pressure P^*. The yield stress Y corresponding to each of the curves is indicated.

mechanical scenario for the pore collapse processes. However, *Curran and Carroll*'s [1979] model seems to have an intrinsic limitation in that it cannot consistently reproduce the yield cap for both hydrostatic and nonhydrostatic loading with the same set of yield parameters.

[49] There are at least three possible reasons for this model limitation. First, while the pores in the carbonate rocks are mostly equant in shape they are not exactly spherical as idealized in the model. Our earlier analysis of the dependence of compressibility on porosity suggests that the pore geometry may deviate from perfectly spherical. We note that there have been recent attempts to develop models taking into account pore shapes other than a sphere [e.g., *Sevostianov and Kachanov*, 2001]. Second, the model assumes an isotropic yield criterion, but the mechanical behavior of sedimentary rocks may be strongly anisotropic and in particular significant mechanical anisotropy may arise from bedding. For example, in the Rothbach sandstone the compactive yield stresses in samples cored perpendicular to bedding are consistently higher than those parallel to bedding [*Wong et al.*, 1997]. Since our samples were all cored perpendicular to bedding, if the limestones have a similar type of anisotropy then it is to be expected that a higher yield stress value is required to fit the triaxial compression data. It would be desirable to conduct a future study on the effect of bedding on compaction and yield in carbonate rocks. Last, the yield condition (2) assumes pressure insensitivity, but the operative mechanisms (especially in the more porous carbonate rocks) probably involve pressure-dependent frictional process. Our microstructure observations on Indiana limestone (Vajdova et al. manuscript in preparation, 2004) as well as observations of others [e.g., *Groshong*, 1974; *Myer et al.*, 1992] indicate cataclastic processes such as fracturing and frictional sliding. It is expected that cataclasis contributes to the yielding besides crystal plasticity.

[50] To address the last issue one may consider the end-member that neglects crystal plasticity and as an alternative considers cataclastic yield described by a pressure-sensitive criterion such as the Mohr-Coulomb [*Bhatt et al.*, 1975] or Drucker-Prager [*Curran and Carroll*, 1979] criterion. Even for such an end-member the analysis is rather involved and beyond the scope of the present study. Nevertheless we are currently investigating this question, guided by our microstructural observations. While the analyses of these end-members can provide useful mechanical constraints, it is likely that pore collapse in the more porous carbonate rocks involves the complex interplay of both cataclastic and crystal plasticity mechanisms. In a fossiliferous limestone such as the Indiana limestone, *Groshong*'s [1974] and our observations (to be presented in a future publication) showed relative grain movements among the fossil fragments and ooids as well as some microcracking, in addition to deformation twinning that develops in the calcite cement. If these mechanisms act to shield the stress concentration from one another then the local stresses required to simultaneously activate them could be higher than that required to active an individual mechanism. While twinning and dislocation slip may enhance the local stress intensity to promote microcracking, they can also effectively inhibit damage development by alleviating the stresses at propagating crack tips and at grain contacts during relative movement [*Fredrich et al.*, 1989]. Furthermore microcracking and the associated stress concentration may be controlled by the grain size, which has not been incorporated into micromechanical models focusing on the influence of porosity. These questions can only be addressed in a quantitative manner by a more elaborate model that explicitly accounts for the coupling of the crystal plasticity and cataclastic mechanisms during pore collapse.

3.6. Transition From Shear-Enhanced Compaction to Dilatancy

[51] *Baud et al.* [2000] interpreted the transition from compactive to dilatant cataclastic flow ($C^{*\prime}$ at Figure 8a, 8b, 8c) as the point at which cumulative dilation due to cracking exceeds the concomitant compaction due to pore collapse. This interpretation is supported by microscopy observations that show evidence of microcracks parallel to σ_1 in samples deformed beyond $C^{*\prime}$. For the Solnhofen limestone since compactive yield involves dislocation slip *Baud et al.* [2000] suggested that crack nucleation arises from tensile stresses induced by dislocation pileup at obstacles like grain boundaries, second-phase particles and nearby dislocations [*Zener*, 1948; *Stroh*, 1957; *Wong*, 1990]. Such a model predicts the critical stress $C^{*\prime}$ to be pressure-independent. Indeed the Solnhofen limestone data show relatively low pressure sensitivity and the stress magnitudes are comparable to the model predictions for dislocation slip.

[52] To what extent can the same model be applied to the more porous carbonate rocks? Since deformation twinning slip may also induce local tensile stress concentration and nucleate cracks [*Olsson and Peng*, 1976; *Fredrich et al.*, 1989], dilatancy associated with $C^{*\prime}$ in the more porous carbonate rocks can arise from a similar mechanism, although it is unclear to what extent the cracks may propagate once they have been nucleated. Some of our microscopy observations on Indiana limestone relevant to this question will be detailed in a future publication.

[53] There is an additional problem in that the $C^{*\prime}$ data for both Tavel and Indiana limestones show relatively strong dependence on the mean stress (Figures 8a and 8b). Indeed in the stress space, they follow trends similar to those for the brittle strength, with the implication that frictional, cataclastic mechanisms play dominant roles in this regime. The transition from compactive to dilatant cataclastic flow was observed in the Lance sandstone, and the data for the critical stress $C^{*\prime}$ also show strong dependence on the mean stress [*Schock et al.*, 1973; *Baud et al.*, 2000].

[54] It should be noted that such a transition can also be accomplished by pursuing a somewhat different stress path. One can first hydrostatically compact the sample to beyond the pore collapse pressure P^*, then reduce the pressure to a lower value before applying the differential stress to ultimately attain dilatant failure. Such a stress path is similar to that commonly used in soil mechanics for studying overconsolidation and its consequence on the mechanical response. This approached has been employed by *Wong et al.* [1992] and *Homand and Shao* [2000] on the Berea sandstone and Lixhe chalk, respectively. For both rocks the critical stresses for onset of dilatancy show strong pressure sensitivity, following a trend in the stress space similar to that in the brittle regime. This also indicates that in the

highly porous chalk frictional, cataclastic mechanisms are dominant.

4. Summary

[55] Our hydrostatic and triaxial compression experiments on Indiana and Tavel limestones show that the phenomenology of dilatant and compactant failure in these porous carbonate rocks is similar to that of the more compact Solnhofen limestone as well as many porous sandstones. Porosity exerts significant influence over the elastic, inelastic and failure properties of the carbonate rocks. The compressibility increases with increasing porosity, and comparison of the laboratory data with theoretical model indicates that the pore geometry deviates somewhat from perfectly spherical.

[56] The brittle strength decreases with increasing porosity. The onset of dilatancy and peak stress of the limestones can be interpreted using a micromechanical model based on sliding wing cracks. The critical stresses for the onset of pore collapse under hydrostatic and nonhydrostatic loadings also decrease with increasing porosity. Experimental data for carbonate rocks with porosities ranging from 3% to 45% can be interpreted using a micromechanical model based on plastic collapse of spherical pores, if the assumption is made that the plastic yield stress decreases with increasing porosity, possibly due to the activation of different crystal plasticity mechanisms at different porosity range. The inference is that mechanical twinning dominates in the more porous limestones and chalk, while dislocation slip is activated in the more compact limestones. The latter mechanism is expected to be sensitive to temperature.

[57] The spherical pore collapse model seems to have an intrinsic limitation in that it cannot consistently reproduce the yield cap for both hydrostatic and nonhydrostatic loadings with the same set of yield parameters. To arrive at better agreement with the laboratory data the model should be modified to account for coupling of crystal plasticity and cataclastic mechanisms such as fracturing and frictional sliding. Nonspherical pore geometry and mechanical anisotropy should also be considered.

[58] **Acknowledgments.** We are grateful to Elisabeth Bemer and Roberto Suarez-Rivera who kindly furnished us with the blocks of the Tavel limestone and Indiana limestone, respectively. We have benefited from discussions with Joanne Fredrich, Alexandre Schubnel, Jian-Fu Shao and Wenlu Zhu as well as critical reviews by Fred Chester and an anonymous reviewer. This research was partially supported by the Office of Basic Energy Sciences, Department of Energy under grant DE-FG02-99ER14996.

References

Ashby, M. F., and C. G. Sammis (1990), The damage mechanics of brittle solids in compression, *Pure Appl. Geophys.*, *133*, 489–521.

Atkinson, B. K., and V. Avdis (1980), Fracture mechanics parameters of some rock-forming minerals determined using an indentation technique, *Int. J. Rock Mech. Min. Sci. Geomech. Abstr.*, *17*, 383–386.

Azeemuddin, M., T. E. Scott, and M. Zaman (1994), Variations in acoustic wave velocity induced during deformation of Ekofisk chalk, *RMC-94–17*, 27 pp., Univ. of Oklahoma, Norman.

Baud, P., A. Schubnel, and T.-f. Wong (2000), Dilatancy, compaction, and failure mode in Solnhofen limestone, *J. Geophys. Res.*, *105*, 19,289–19,303.

Berner, R. A. (1980), *Early Diagenesis*, 237 pp., Princeton Univ. Press, Princeton, N.J.

Bhatt, J. J., M. M. Carroll, and J. F. Schatz (1975), A spherical model calculation for volumetric response of porous rocks, *J. Appl. Mech.*, *42*, 363–368.

Biot, M. A. (1941), General theory of three-dimensional consolidation, *J. Appl. Phys.*, *12*, 155–164.

Boozer, G. D., K. H. Hiller, and S. Serdengecti (1962), Effects of pore fluids on the deformation behavior of rocks subjected to triaxial compression, in *5th Symposium on Rock Mechanics*, edited by C. Fairhurst, Pergamon, New York.

Boutéca, M., J.-P. Sarda, and F. Schneider (1996), Subsidence induced by the production of fluids, *Rev. Inst. Fr. Pet.*, *51*, 349–379.

Brace, W. F. (1978), Volume changes during fracture and frictional sliding: A review, *Pure Appl. Geophys.*, *116*, 603–614.

Brace, W. F., and D. K. Riley (1972), Static uniaxial deformation of 15 rocks to 30 kb, *Int. J. Rock Mech. Min. Sci.*, *9*, 271–288.

Carroll, M. M. (1980), Compaction of dry or fluid-filled porous materials, *J. Eng. Mech.*, *106*(EM5), 969–990.

Choquette, P. W., and N. P. James (1986), Diagenesis in limestones: The deep burial environment, *Geosci. Can.*, *14*, 3–35.

Cotterell, B., and J. R. Rice (1980), Slightly curved or kinked cracks, *Int. J. Fract.*, *16*, 155–169.

Coyner, K. B. (1984), Effects of stress, pore pressure, and pore fluids on bulk strain, velocity, and permeability of rocks, Ph. D. thesis, Mass. Inst. of Technol., Cambridge.

Curran, J. H., and M. M. Carroll (1979), Shear stress enhancement of void compaction, *J. Geophys. Res.*, *84*, 1105–1112.

Dahou, A., J. F. Shao, and M. Bederiat (1995), Experimental and numerical investigations on transient creep of porous chalk, *Mech. Mat.*, *21*, 147–158.

David, C., T.-f. Wong, W. Zhu, and J. Zhang (1994), Laboratory measurement of compaction-induced permeability change in porous rock: Implications for the generation and maintenance of pore pressure excess in the crust, *Pure Appl. Geophys.*, *143*, 425–456.

Elliot, G. M., and E. T. Brown (1986), Further development of a plasticity approach to yield in porous rocks, *Int. J. Rock Mech. Sci. Geomech. Abstr.*, *23*, 151–156.

Ewy, R. T., and N. G. W. Cook (1990), Deformation and fracture around cylindrical opening in rocks, I. Observations and analysis of deformations, *Int. J. Rock Mech. Min. Sci.*, *27*, 387–407.

Fabre, D., and J. Gustkiewicz (1997), Poroelastic properties of limestones and sandstones under hydrostatic conditions, *Int. J. Rock Mech. Min. Sci.*, *34*, 127–134.

Fisher, G. J., and M. S. Paterson (1989), Dilatancy during rock deformation at high temperatures and pressures, *J. Geophys. Res.*, *94*, 17,607–17,618.

Fredrich, J. T., B. Evans, and T.-f. Wong (1989), Micromechanics of the brittle to plastic transition in Carrara marble, *J. Geophys. Res.*, *94*, 4129–4145.

Fredrich, J., B. Evans, and T.-f. Wong (1990), Effects of grain size on brittle and semi-brittle strength: Implications for micromechanical modelling of failure in compression, *J. Geophys. Res.*, *95*, 10,907–10,920.

Fredrich, J. T., J. G. Arguello, G. L. Deitrick, and E. P. deRouffignac (2000), Geomechanical modeling of reservoir compaction, surface subsidence, and casing damage at the Belridge diatomite field, *SPE Reservoir Eval. Eng.*, *3*, 348–359.

Geertsma, J. (1973), Land subsidence above compacting oil and gas reservoirs, *J. Pet. Technol.*, *25*, 734–744.

Goldsmith, A. S. (1989), Permeability decline and compressibility in sandstone reservoir rocks, in *Rock at Great Depth*, edited by V. Maury and D. Fourmaintraux, pp. 923–928, A. A. Balkema, Brookfield, Vt.

Grasso, J. R., and G. Wittlinger (1990), Ten years of seismic monitoring over a gas field area, *Bull. Seismol. Soc. Am.*, *80*, 450–473.

Griggs, D. T., F. J. Turner, and H. C. Heard (1960), Deformation of rocks at 500° to 800°C, in *Rock Deformation*, edited by D. T. Griggs and J. Handin, *Mem. Geol. Soc. Am.*, *79*, 39–104.

Groshong, R. H. (1974), Experimental test of least-squares strain gage calculation using twinned calcite, *Geol. Soc. Am. Bull.*, *85*, 1855–1864.

Hart, D. J., and H. F. Wang (1995), Laboratory measurements of a complete set of poroelastic moduli of Berea sandstone and Indiana limestone, *J. Geophys. Res.*, *100*, 17,741–17,751.

Heard, H. C. (1960), Transition from brittle fracture to ductile flow in Solnhofen limestone as a function of temperature, confining pressure and interstitial fluid pressure, in *Rock Deformation*, edited by D. T. Griggs and J. Handin, *Mem. Geol. Soc. Am*, *79*, 193–226.

Hoagland, R. G., G. T. Hahn, and A. R. Rosenfield (1973), Influence of microstructure on fracture propagation in rock, *Rock Mech.*, *5*, 77–106.

Homand, S., and J. F. Shao (2000), Mechanical behaviour of a porous chalk and effect of saturating fluid, *Mech. Cohes. Frict. Mater.*, *5*, 583–606.

Horii, H., and S. Nemat-Nasser (1986), Brittle failure in compression: Splitting, faulting and brittle ductile transition, *Philos. Trans. R. Soc. London Ser. A*, *319*, 337–374.

Jones, M. E., and M. J. Leddra (1989), Compaction and flow of porous rocks at depth, in *Rocks at Great Depth*, edited by V. Maury and D. Fourmaintraux, pp. 891–898, A. A. Balkema, Brookfield, Vt.

Kachanov, M. (1994), Elastic solids with many cracks and related problems, *Adv. Appl. Mech.*, *30*, 259–445.

Kemeny, J. M., and N. G. W. Cook (1991), Micromechanics of deformation in rocks, in *Toughening Mechanisms in Quasi-Brittle Materials*, edited by S. P. Shah, pp. 155–188, Kluwer Acad., Norwell, Mass.

Laurent, J., M. Boutéca, J.-P. Sarda, and D. Bary (1993), Pore-pressure influence in the poroelastic behavior of rocks: Experimental studies and results, *SPE Form. Eval.*, *8*, 117–122.

Longuemare, P., A. Onaisi, and I. Shahrour (1995), Elaboration of an elasto-plastic model for high porosity chalks, *Rev. Inst. Fr. Pet.*, *50*, 599–609.

Mackenzie, J. K. (1950), The elastic constants of a solid containing spherical holes, *Proc. Phys. Soc. London*, *63*, 2–11.

Mwar, S., M. Zaman, D. W. Stearns, and J.-C. Roegiers (1994), Pore collapse mechanisms in Cordoba Cream limestone, *Proc. North Am. Rock Mech. Symp.*, *1*, 767–773.

Myer, L. R., J. Kemeny, N. G. W. Cook, R. Ewy, R. Suarez, and Z. Zheng (1992), Extensile cracking in porous rock under differential compressive stress, *Appl. Mech. Rev.*, *45*, 263–280.

Nagel, N. B. (2001), Compaction and subsidence issues within the petroleum industry: From Wilmington to Ekofisk and beyond, *Phys. Chem. Earth Part A*, *26*, 3–14.

Olsson, W. A., and S. S. Peng (1976), Microcrack nucleation in marble, *Int. J. Rock Mech. Min. Sci Geomech. Abstr.*, *13*, 53–59.

Paterson, M. S. (1958), Experimental deformation and faulting in Wombeyan marble, *Geol. Soc. Am. Bull.*, *69*, 465–476.

Paterson, M. S. (1958), *Experimental Rock Deformation: The Brittle Field*, Springer-Verlag, New York.

Peck, L., C. C. Barton, and R. B. Gordon (1985), Microstructure and the resistance of rock to tensile fracture, *J. Geophys. Res.*, *90*, 1533–1546.

Rhett, D. W., and L. W. Teufel (1992), Stress path dependence of matrix permeability of North Sea sandstone reservoir rock, *Proc. U.S. Rock Mech. Symp.*, *33*, 345–354.

Risnes, R., C. N. Kristensen, and M. A. Andersen (1996), Triaxial tests on high porosity chalk with different saturating fluids, paper presented at Fifth North Sea Chalk Symposium, Reims, France.

Robertson, E. C. (1955), Experimental study of the strength of rocks, *Bull. Geol. Soc. Am.*, *66*, 1275–1314.

Robinson, R. H. (1959), The effect of pore and confining pressure on the failure process in sedimentary rocks, *Colo. Sch. Mines Q.*, *54*, 177–199.

Rowe, K. J., and E. H. Rutter (1990), Paleostress estimation using calcite twinning: Experimental calibration and application to nature, *J. Struct. Geol.*, *12*, 1–17.

Rutter, E. H. (1972), The influence of interstitial water on the rheological behaviour of calcite rocks, *Tectonophysics*, *14*, 13–33.

Rutter, E. H. (1974), The influence of temperature, strain rate and interstitial water in the experimental deformation of calcite rocks, *Tectonophysics*, *22*, 331–334.

Schmidt, R. A. (1976), Fracture-toughness testing of limestone, *Exp. Mech.*, *16*, 161–167.

Schock, R. N., H. C. Heard, and D. R. Stephens (1973), Stress-strain behavior of a granodiorite and two graywackes on compression to 20 kilobars, *J. Geophys. Res.*, *78*, 5922–5941.

Schwartz, A. E. (1964), Failure of rock in the triaxial shear test, in *Proceedings 6th Symposium on Rock Mechanics*, edited by E. M. Spokes and C. R. Christensen, pp. 101–151, Univ. of Mo., St. Louis.

Segall, P. (1989), Earthquakes triggered by fluid extraction, *Geology*, *17*, 942–946.

Segall, P., and S. D. Fitzgerald (1998), A note on induced stress changes in hydrocarbon and geothermal reservoirs, *Tectonophysics*, *289*, 117–128.

Sevostianov, I., and M. Kachanov (2001), On the yield condition for anisotropic porous materials, *Mater. Sci. Eng.*, *A313*, 1–15.

Simmons, G., and H. F. Wang (1971), *Single Crystal Elastic Constants and Calculated Aggregate Properties*, Mass. Inst. Technol. Press, Cambridge.

Smits, R. M. M., J. A. de Waal, and J. F. C. van Kooten (1988), Prediction of abrupt reservoir compaction and surface subsidence caused by pore collapse in carbonates, *SPE Form. Eval.*, *3*, 340–346.

Stroh, A. N. (1957), A theory of the fracture of metals, *Adv. Phys.*, *6*, 418–465.

Suarez-Rivera, F. R., N. G. W. Cook, G. A. Cooper, and Z. Zheng (1990), Indentation by pore collapse in porous rocks, in *Rock Mechanics Contributions and Challenges: Proceedings of the 31st U.S. Symposium on Rock Mechanics*, edited by W. A. Hustrulid and G. A. Johnson, pp. 653–660, A. A. Balkema, Brookfield, Vt.

Tapponier, P., and W. F. Brace (1976), Development of stress-induced microcracks in Westerly granite, *Int. J. Rock Mech. Min. Sci. Geomech Abstr.*, *13*, 103–112.

Teufel, L. W., D. W. Rhett, and H. E. Farrell (1991), Effect of reservoir depletion and pore pressure drawdown on in situ stress and deformation in the Ekofisk field, North Sea, *Proc. U.S. Rock Mechanics Symp.*, *32*, 63–72.

Turner, F. J., D. T. Griggs, and H. C. Heard (1954), Experimental deformation of calcite crystals, *Geol. Soc. Am. Bull.*, *65*, 883–934.

Vernik, L., M. Bruno, and C. Bovberg (1993), Empirical relations between compressive strength and porosity of siliciclastic rocks, *Int. J. Rock Mech. Min. Sci.*, *30*, 677–680.

Vincké, O., M. J. Boutéca, J. M. Piau, and D. Fourmaintraux (1998), Study of the effective stress at failure, in *Poromechanics, A Tribute to Maurice A. Biot*, edited by J.-F. Thimus et al., pp. 635–639, A. A. Balkema, Brookfield, Vt.

Walsh, J. B. (1965), The effect of cracks on the compressibility of rocks, *J. Geophys. Res.*, *70*, 381–389.

Walsh, J. B. (1980), Static deformation of rock, *J. Eng. Mech.*, *106*, 1005–1019.

Wawersik, W. R., and C. Fairhurst (1970), A study of brittle rock fracture in laboratory compression experiments, *Int. J. Rock Mech. Min. Sci.*, *7*, 561–575.

Wong, T.-f. (1982), Micromechanics of faulting in Westerly granite, *Int. J. Rock Mech. Min. Sci. Geomech. Abstr.*, *19*, 49–64.

Wong, T.-f. (1990), A note on propagation behavior of a crack nucleated by a dislocation pileup, *J. Geophys. Res.*, *95*, 8639–8646.

Wong, T.-f., and P. Baud (1999), Mechanical compaction of porous sandstone, *Oil Gas Sci. Technol.*, *54*, 715–727.

Wong, T.-f., H. Szeto, and J. Zhang (1992), Effect of loading path and porosity on the failure mode of porous rocks, *Appl. Mech. Rev.*, *45*, 281–293.

Wong, T.-f., C. David, and W. Zhu (1997), The transition from brittle faulting to cataclastic flow in porous sandstones: Mechanical deformation, *J. Geophys. Res.*, *102*, 3009–3025.

Zener, C. (1948), The micro-mechanism of fracture, in *Fracture of Metals*, edited by F. Johnson, W. P. Roop, and R. T. Bayles, pp. 3–31, Am. Soc. for Metals, Cleveland, Ohio.

Zhang, J., T.-f. Wong, and D. M. Davis (1990), Micromechanics of pressure-induced grain crushing in porous rocks, *J. Geophys. Res.*, *95*, 341–352.

Zheng, Z., N. G. W. Cook, and L. R. Myer (1989), Stress induced microcrack geometry at failure in unconfined and confined axial compressive tests, *Proc. U. S. Rock Mech. Symp.*, *30*, 749–756.

Zimmerman, R. W. (1991), *Compressibility of Sandstones*, 173 pp., Elsevier Sci., New York.

P. Baud, Institut de Physique du Globe, Ecole et Observatoire des Sciences de la Terre (CNRS/ULP), 5 rue Descartes, 67084 Strasbourg, France.

V. Vajdova and T.-f. Wong, Department of Geosciences, State University of New York at Stony Brook, Stony Brook, NY 11794-2100, USA. (vvajdova@ic.sunysb.edu)